Eur. Phys. J. D (2023)77:90
https://doi.org/10.1140/epjd/s10053-023-00673-x

THE EUROPEAN PHYSICAL JOURNAL D

Regular Article – Optical Phenomena and Photonics

Broadband supercontinuum generation in a square lattice photonic crystal fiber with C_6H_6-core using low pump power

Bao Tran Le Tran[a] and Lanh Chu Van[b]

Department of Physics, Vinh University, 182 Le Duan, Vinh City 43100, Vietnam

Received 31 December 2022 / Accepted 16 May 2023

Abstract We numerically investigate the near-zero flat dispersion supercontinuum generation (SCG) in hollow-core square photonic crystal fibers (PCFs) with benzene-core (C_6H_6). Different air hole sizes in the rings result in a structure that simultaneously optimizes fiber properties. A unique combination between low all-normal dispersion and high nonlinearity enables low-noise SC covering 0.72–1.76 μm. This requires 0.45 kW of peak power realized by ultrafast standard erbium-fiber laser with 40 fs pulse duration. PCF with an anomalous dispersion enables SCG to cover the spectral range of 0.8–3.95 μm at 1.55 μm when pumped by power pulses less than 0.55 kW. This is a much lower input power level than previously for SCG with bandwidths greater than one octave in liquid-core structures. Our results show that liquid-core fibers are a promising method to scale the SC spectrum with pump lasers with limited peak power per pulse. Such fibers are often used in frequency measurement, optical communication, and high-speed nonlinear imaging.

1 Introduction

Research fields associated with photonic crystal fiber (PCF) technology are thriving to revolutionize nonlinear devices by replacing optical fibers shortly. Although performing very well in telecommunications and non-telecommunication applications, classical optical fibers often have harsh rules regarding their geometry that cause light to transmit over small distances [1]. PCF introduces a new way to trap light with great flexibility in varying design parameters to adjust fiber optical characteristics such as nonlinearity, numerical aperture, dispersion, effective mode area, transmission constant, etc. This special property of PCF has underpinned many recent advances in fiber sensing, supercontinuum generation (SCG), laser technology, and fiber amplification [2, 3]. Among them, the phenomenon of SCG occurs due to the combination of managed dispersion and promoted nonlinearity and has led to many studies due to the variety of this type of application [3–5]. In this context, the behavior of the flat dispersion fiber becomes an important requirement. The flatter and near-zero the dispersion, the more effective the SCG [6].

It is worth noting that the reduced effective mode area of mode propagating in PCF increases the Kerr nonlinear effect compared to standard fiber. This is based on the relationship [6]:

$$\gamma = 2\pi n_2/\gamma A_{\text{eff}}. \tag{1}$$

Up to now, there are various techniques by which effective mode area, as well as other characteristics of PCF, can be designed and modified for a particular application. Most of proposed techniques are based on changing the shape of the fiber, i.e., the diameter of air holes, the hole-to-hole distance, and the number and geometric distribution of the air holes around the core [7–9]. Excellent controllability in chromatic dispersion, single-mode wavelength range, nonlinearity coefficient, attenuation, and effective mode area has been studied numerically for the past 10 years and introduced in individual works [8–11]. PCFs reported in the following years [12–14] significantly improved when all their characteristics were investigated, but the authors have not yet applied the results obtained to the SCG. Recently, pulse compression and SCG have been obtained using hexagonal PCFs in different wavelength regimes in the near- and mid-infrared bands. Although the good potential of the hexagonal lattice has been confirmed

[a] e-mail: letranbaotran212@gmail.com
[b] e-mail: chuvanlanh@vinhuni.edu.vn (corresponding author)

Published online: 31 May 2023

in several papers [3, 15] due to the strong enhancement of nonlinearity, especially the near-zero flat dispersion curve than other types of lattice, the spectral flatness, in this case, is not good. Meanwhile, square lattice PCF both exhibits sufficient flat and negative dispersion coefficients and can also minimize the total loss during propagation [12]. It can also be useful if applied as a pigtail fiber of an integrated optical device with a square or rectangular cross-section [16]. Additionally, square PCF also helps scientists to achieve high birefringence [16], wide single-mode active region [17], dispersion compensation [16], and high nonlinearity [12] with all group velocity dispersion for SCG light source design.

According to formula (1), another method to achieve large nonlinear parameters in optical fiber is to choose materials with a large nonlinear coefficient (n_2). In this approach, one fills the hollow fiber with selective liquid to form a liquid-core photonic fiber. These organic solvents are transparent in the visible and near-infrared (NIR) ranges; hence, stimulated Raman scattering and broadband SCG are easily observed with small input power or low energy pulses [7, 15, 18–22]. Compared with silica (SiO_2), the nonlinear liquid exhibits a much higher nonlinear refractive index, one of which is comparable to that of a solid core fiber from soft glass. The use of soft glass fibers such as silicate, tellurite, and chalcogenide glass provides many wide-bandwidth transmission windows into the mid-infrared (MIR) range, and the generation of SC is significantly shorter in length. However, these glasses suffer from mechanical limitations, laser power handling, dispersion slope in NIR, incompatibility with SiO_2 for fusion splicing, and often require complex sources of laser systems [23, 24]. In contrast, the form of infiltration into the PCF core with liquids leading to additional degrees of freedom overcomes these limitations and enhances the range of possible applications [25].

Along with the requirements set on the nonlinear refractive index, there is also interest in whether selected liquids are environmentally friendly. Generally, fluids with higher nonlinear refractive index are more toxic, such as carbon disulfide (CS_2) [21]. For this reason, other liquids (toluene, nitrobenzene, benzene, carbon tetrachloride, or chloroform) are preferred for practical applications. Benzene (C_6H_6) is one of the most interesting options herein as it is less toxic when compared to CS_2 and is widely used to make some types of rubbers, adhesives, dyes, cleaning products, pesticides, and gasoline. Nonlinear refractive index $n_2 = 168 \times 10^{-20}$ m^2/W at 1.064 μm wavelength is 60 times greater than SiO_2. This value is comparable to the nonlinearity of nitrobenzene and toluene and is much greater than the one of chloroform and carbon tetrachloride. Another advantage of the C_6H_6 is that the 0.5 μm to 1.4 μm wide transparent window allows free soliton displacement, self-phase modulation (SPM), and optical wave breaking (OWB) without attenuating some parts of the spectrum [15, 26]. Recently, Lanh et al. [15] demonstrated that an SC broader than two octaves (4:1) can be efficiently induced in C_6H_6-core PCFs with a fiber length shorter than 1 cm based on an energy femtosecond pulse $\leq 2n$J. However, an economic trade-off exists, namely that the input peak power (ratio of pulse energy to pulse width) is quite high and the spectral range is still limited. In addition, investigated PCFs have air holes with the same diameter arranged in a regular pattern throughout the micro-structured cladding. We required different air hole diameters to realize ultra-flat dispersion, small loss, and high nonlinear coefficient over a long-wavelength window [27]. Indeed, C_6H_6-PCFs with different lattice types have been designed with heterogeneous air hole rings optimized for simultaneous dispersion and loss characteristics for broad SCG [28]. They achieve SC bandwidths of 0.786 μm, 0.897 μm, and 0.977 μm for circular, square, and hexagonal lattices, respectively, with 0.11 kW low pump power and 40 fs pulse width. It is worth mentioning that the above publication only compares the SC spectrum in the all-normal dispersion (ANDi SCG), where SCG process is mainly controlled by the SPM and OWB. One reason for this is that the coherence of SC generated is very high. However, the superior coherence obtained at the expense of narrow spectral bandwidth and large peak power is the main disadvantage of ANDi SCG. The emergence of new optical pulses generated from elementary soliton fission when pumping in an anomalous dispersion regime harms the SC coherence. Notwithstanding, the spectrum width, in this case, is extremely wide beyond the limits of ANDi SCG [21].

In this work, we investigate for the first time the simultaneous SCG in both dispersion regimes in the SiO_2-based PCF with a square lattice. The fiber core is filled with C_6H_6 thanks to a pump system. Our fiber design has achieved the following improvements:

1. Near-zero flat dispersion with a small effective mode area and high nonlinearity over a wide range of the wavelength.
2. SC shows a large expansion while the peak power is very low and the propagation length is short.

All the numerical studies reported in this paper are as follows: First, we briefly describe the simulation method and set relevant parameters of the proposed structure. The strategy of optimizing optical characteristics based on adjusting the air hole diameters arranged around the core is mentioned shortly afterward. The next section presents the theory of the SCG model and analyzes the effect of different pulse parameters on SCG performance. SC spans two octaves and the flat profile is finally proved when all factors are considered.

2 Basic theory and equations

By finite-element method (FEM) with an anisotropic perfectly matched layer, we obtain the effective mode area, dispersion coefficient, and nonlinear coefficient. In

PCF, changing the lattice constant and air hole diameter can significantly vary all optical parameters, but the physical realization remains a real challenge. The background material is SiO_2, whose refractive index is determined using Sellmeier equation [29, 30]:

$$n^2_{SiO_2}(\lambda) = 1 + \frac{0.6694226\lambda^2}{\lambda^2 - 4.4801 \times 10^{-3}} + \frac{0.4345839\lambda^2}{\lambda^2 - 1.3285 \times 10^{-2}} + \frac{0.8716947\lambda^2}{\lambda^2 - 95.341482}, \quad (2)$$

where λ is the wavelength and n is the refractive index of the material. The effective index is given as:

$$n_{\text{eff}} = \lambda\beta/2\pi, \quad (3)$$

where β is the propagation constant. Chromatic dispersion plays a major key because of which the propagating pulse broadens along the fiber length. It is the combination of waveguide dispersion (D_w) and material dispersion (D_m) and is given by the relationship of [17]:

$$D(\lambda) = D_m(\lambda) + D_w(\lambda) = -(\lambda/c) \times \left(\partial^2 \text{Re}[n_{\text{eff}}]/\partial\lambda^2\right), \quad (4)$$

where $\text{Re}[n_{\text{eff}}]$ is the real part of the modal refractive index.

Technically, the production of white light by high-intensity pulses is called SC. This process has the contribution of SPM, cross-phase modulation (XPM), OWB, stimulated Raman scattering, and four-wave mixing (FWM), etc. [31]. Depending on optical properties such as fiber nonlinearity, center wavelength, pulse width, and peak power of the laser sources, the dispersion characteristics govern physical processes. Optical solitons dominate in the femtosecond range. The nonlinear Schrödinger equation (NLSE) describes the light wave propagation through a medium given by [32]:

$$\frac{\partial}{\partial_z}A(z, T) = -\frac{\alpha}{2}A(z, T) + \sum_{n\geq 2}\beta_n \frac{i^{n+1}}{n!}\frac{\partial^n}{\partial t^n}A(z, T) + i\gamma\left(1 + \frac{i}{\omega_0}\frac{\partial}{\partial T}\right)\int_{-\infty}^{+\infty} R(T')\left|A(z, T - T')\right|^2 dT', \quad (5)$$

where $A(z, T)$ is the electric field envelop, α represents the attenuation, and β_n is the nth-order dispersion at center frequency ω_0. $R(T)$ is the Raman response function defined as [32]:

$$R(t) = (1 - f_r)\delta(T) + f_r h_r(T), \quad (6)$$

and

$$h_r(T) = \left((\tau_1^2 + \tau_2^2)/(\tau_1\tau_2^2)\right). \quad (7)$$

This equation is solved using a simple and exact split-step Fourier transform method. A hyperbolic secant pulse is used for the SCG simulations [32]:

$$A(z, T) = \sqrt{P_0}\text{sech}(T/T_0), \quad (8)$$

where P_0 is the peak power and T_0 is the width of the input pulse. SCG is initially dominated by modulation instability (MI) and then by SPM in ultrashort pulses, giving rise to soliton dynamics in the anomalous dispersion regime. The process of decaying a pulse of sufficient peak power into subpulses is called soliton fission [6]. The soliton order N is determined by $N^2 = L_D/L_{NL}$, where L_D is the dispersive length and L_{NL} is the nonlinear length.

3 Design of C_6H_6-core PCF structure

Figure 1a shows a PCF with eight rings of air holes arranged in a square lattice. The distance between two centers of adjacent air holes is called the lattice constant (Λ). If the air hole diameters d of the outer rings is fixed and the diameter of air hole in the first ring near the center is changed, the air filling ratio d_1/Λ will be different. Here we also consider filling the central hollow core with highly nonlinear refractive index C_6H_6 and the advantages shown in the previous section. This is experimentally possible thanks to a laser writing technique that integrates a microfluidic pumping system to fill the core with liquid [31, 33]. The light is well confined in the C_6H_6 core and the diameter of the core is given by the equation $D_{\text{core}} = 2\Lambda - 1.1d_1$ to ensure coupling efficiency with standard fibers (Fig. 1b).

In contrast to the SiO_2 substrate, the linear refractive index of C_6H_6 is calculated using the Cauchy equation (Eq. 9). From the plot of the real component of the refractive indices of C_6H_6 and SiO_2 in Fig. 2, we can conclude that the C_6H_6-PCF behaves like conventional optical fibers because the refractive index of C_6H_6 is always higher than SiO_2. On the other hand, the value of the imaginary part of the linear refractive index k was also experimentally measured using the sample in a standard 1 cm cuvette as shown in Fig. 3 [15]:

$$n^2_{C_6H_6}(\lambda) = 2.170184597 + 0.00593990\lambda^2 + \frac{0.023034640}{\lambda^2} + \frac{0.000499485}{\lambda^4} + \frac{0.000178796}{\lambda^6}. \quad (9)$$

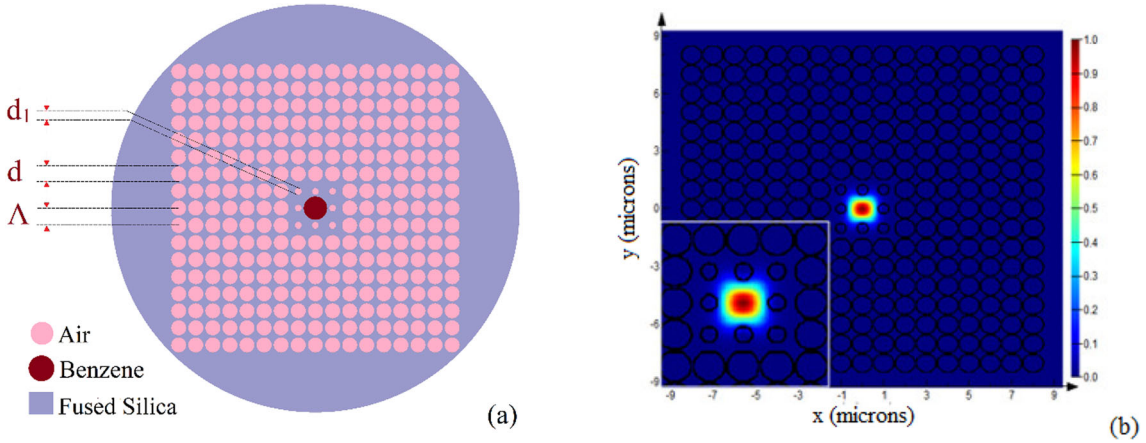

Fig. 1 **a** The geometrical structure and **b** intensity distribution of C_6H_6-core PCF with a square lattice

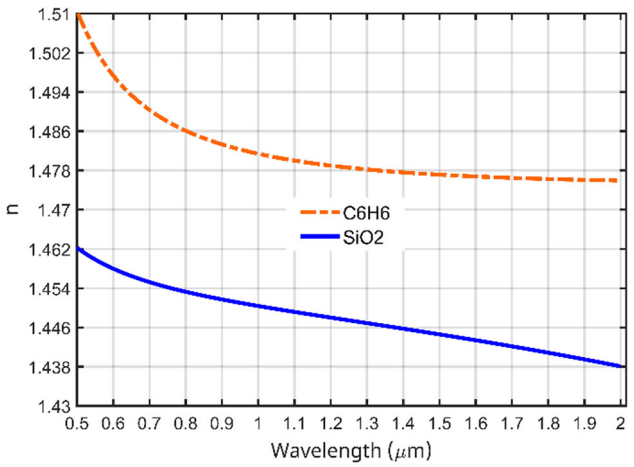

Fig. 2 The real part of the refractive index of SiO_2 and C_6H_6

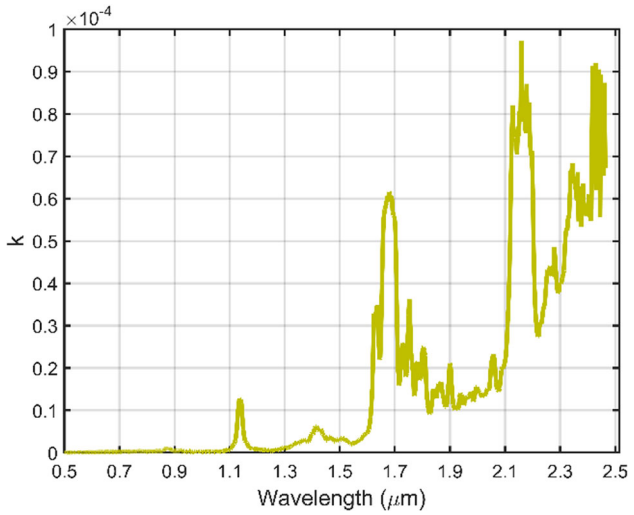

Fig. 3 The imaginary part of the linear refractive index k of C_6H_6

4 Simulation results of C_6H_6-PCF and discussion

4.1 Characteristics of chromatic dispersion, effective mode area, and nonlinear coefficients of the proposed structure

Figure 4a–c shows the chromatic dispersion, effective area, and nonlinear coefficient respectively for the proposed PCFs. In this case, only two optimal fibers with near-zero flat dispersion are chosen, with their parameters specifically noted in the figure. The first structure, $\#F_1$, exhibits all-normal dispersion from the part of the visible to NIR wavelength region and is pumped at 1.3 μm; its dispersion is − 20 ps nm^{-1} km^{-1}. Structure $\#F_2$ has a ZDW at about 1.549 μm with a positive dispersion profile. The dispersion value is equal to 0.03 ps nm^{-1} km^{-1} at 1.55 μm wavelength of the input pulse (λ_p). It can be observed that the A_{eff} curve of the fiber increases with increasing wavelength. Due to its larger core diameter (D_{core} = 4.175 μm), the effective mode area of $\#F_2$ fiber is larger than that of $\#F_1$ at all wavelengths. The nonlinear coefficients of the PCF have opposite trends. It is inversely proportional to A_{eff} according to Eq. (1) and thus decreases with increasing wavelength. The larger the effective mode area, the weaker the nonlinear effects. As a result, the small-core $\#F_1$ fiber (D_{core} = 1.285 μm) has more nonlinearity than $\#F_2$. A high nonlinear PCF is most desirable for SCG with low input energies. At 1.3 μm, the nonlinear coefficient of $\#F_1$ is equal to 5390 W^{-1}·km^{-1}. The figure for $\#F_2$ is 859.79 W^{-1} km^{-1} at 1.55 μm. The A_{eff} values of the two fibers are 1.84 μm^2 and 11.54 μm^2, respectively. Clearly, the nonlinearity is enhanced by falling the core diameter to decrease the effective area and increase n_2 of the material.

Table 1 lists the dispersion, effective mode area, nonlinear coefficients, lattice constant, filling factor, and core diameter used in PCF design. The PCF structure in the reference [34] complicates the design process, different diameters in the first three rings from the core

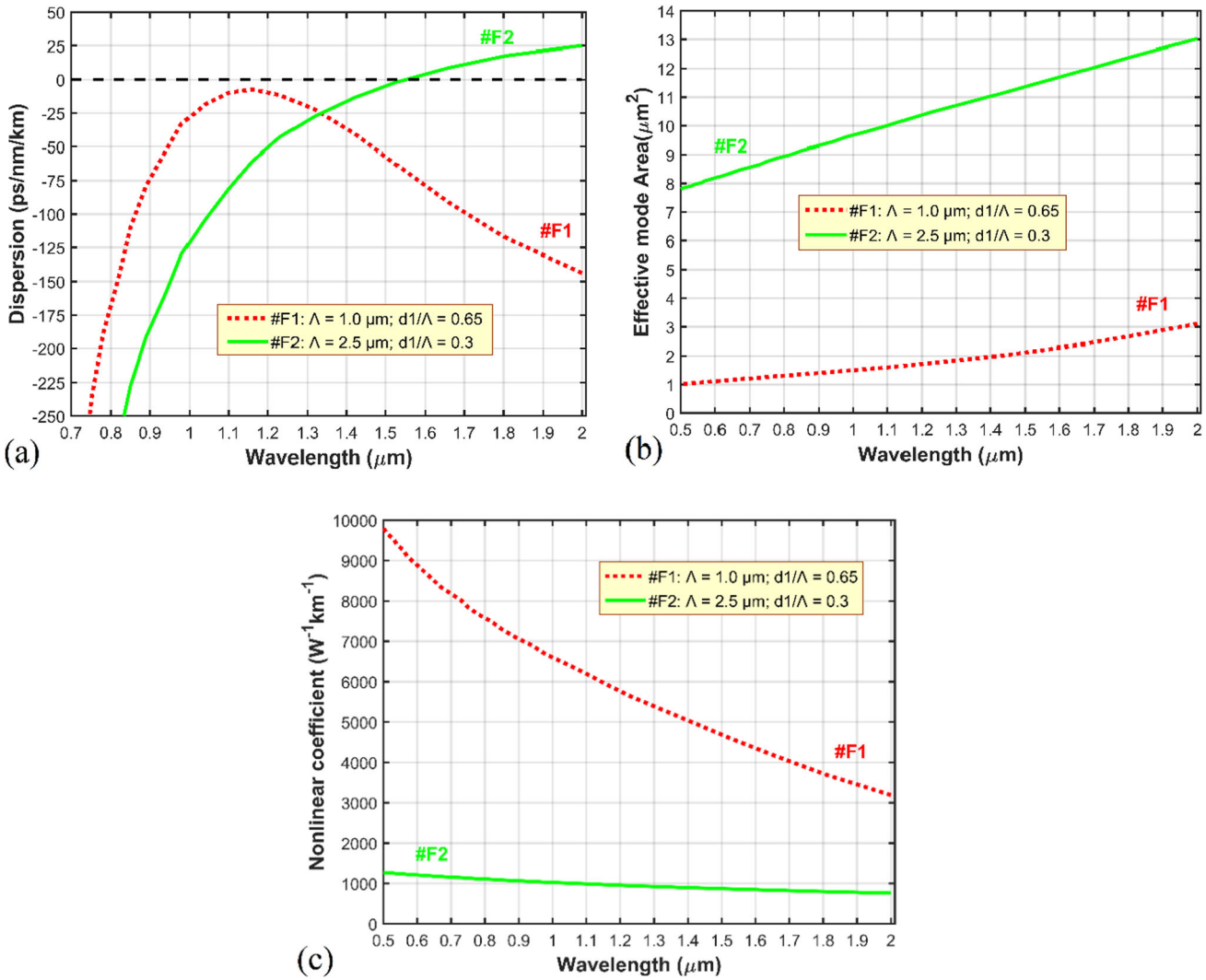

Fig. 4 Characteristics of the fundamental mode for the proposed PCFs. **a** Chromatic dispersion, **b** effective mode area, and **c** nonlinear coefficient

are required to achieve near-zero ultra-flat dispersion. The PCF [34] shows a smaller dispersion compared to PCF proposed, but it is very difficult to generate experimentally. Moreover, compared with the PCFs in [7, 18, 20], our PCFs exhibit flatter chromatic dispersion variation, smaller effective mode area, and higher nonlinearity. Note that SCG efficiency is not high for low nonlinear PCFs [6].

4.2 Detailed analysis of dispersion characteristics for obtaining optimum structures

As mentioned earlier, PCF properties such as dispersion, effective mode area, and nonlinear coefficients can be approximated as the cross-section of the fiber becomes a Yee's lattice structure. For points lying on the surface between two media, an index averaging technique is used for the cells across the interface. This is a change in optical fiber properties due to structural parameters that vary very slightly depending on fabrication. Stack-and-draw fiber method has an error of about 50 nm; thus, this is perfectly suitable for PCF fabrication [35]. For this reason, we did not use optimization algorithms, e.g., genetic algorithms or particle swarm optimization. Optimization algorithms yield structures with better optical properties. However, it requires more simulation time. A simpler method was applied based on the optimization of dispersion characteristics. First, a lattice constant $\Lambda = 1.0$ μm is chosen to maintain a small-core diameter of the fiber. Next, vary the value of d_1/Λ between 0.3 and 0.8 in steps of 0.05 and examine the dispersion curve. From Fig. 5a, we can see that changing the filling factor dramatically changes the dispersion position. A diversity of dispersion properties, including normal and anomalous states along with the existence of zero dispersion wavelengths, is found due to the dominance of waveguide dispersion [18]. In this way, we can obtain suitable dispersion profiles for generating coherent and non-coherent SC with

Table 1 Optical characteristics of the proposed PCFs and other flattened dispersion structures

PCFs	D (ps·nm^{-1}·km^{-1})	A_{eff} (μm^2)	γ (W^{-1} km^{-1})	λ_{p} (μm)	Design parameters		
					Λ (μm)	d_1/Λ	D_{core} (μm)
Ref [7]	7.6	4.48	440	0.92	2.0	0.65	2.57
Ref [18]	1.52	10.497	889.839	1.56	2.5	0.3	4.46
Ref [20]	− 31.8	1.38	2220	1.15	1.0	0.65	1.285
Ref [34]	− 2.249	9.9394	45.15	2.8	1.8	0.45	2.72
#F$_1$	− 20	1.84	5390	1.3	1.0	0.65	1.285
#F$_2$	0.03	11.54	859.79	1.55	2.5	0.3	4.175

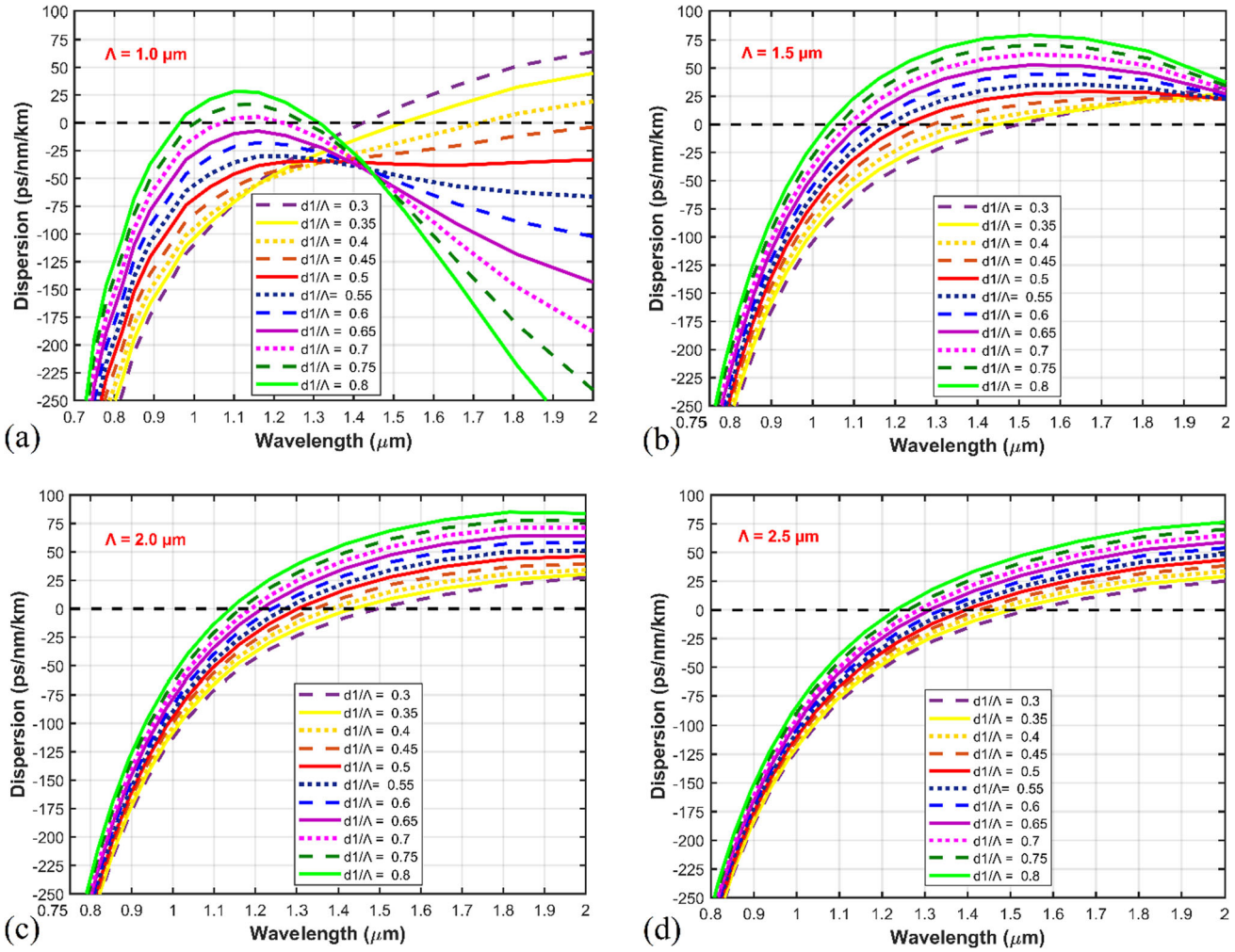

Fig. 5 Dispersion characteristics of the C_6H_6-filled PCFs for $d_1/\Lambda = 0.3 \div 0.8$ and various lattice constants. **a** $\Lambda = 1.0$ μm, **b** $\Lambda = 1.5$ μm, **c** $\Lambda = 2.0$ μm, and **d** $\Lambda = 2.5$ μm

standard fiber femtosecond lasers. Then, change Λ and d_1/Λ to reach the anomalous dispersion, as shown in Fig. 5b–d. Increasing the PCF Λ changes the dispersion regime and decreases the slope of the D curves. In particular, all PCFs with $\Lambda > 1.5$ μm exhibited anomalous dispersion at wavelengths greater than 1 μm, and they possess ZDW. Varying d_1/Λ and keeping the d/Λ value constant have a large impact on the dispersion characteristic. Observing the dispersion curve in Fig. 5, we choose parameters that correspond to a flat, near-zero dispersion curve to generate an ultra-wideband SC. A fiber with$\Lambda = 1.0$ μm and $d_1/\Lambda = 0.65$ is a good candidate for all-normal dispersion, as its peak is asymptotic to the zero dispersion curve. For the anomalous dispersion, we compare three curves that satisfy the above

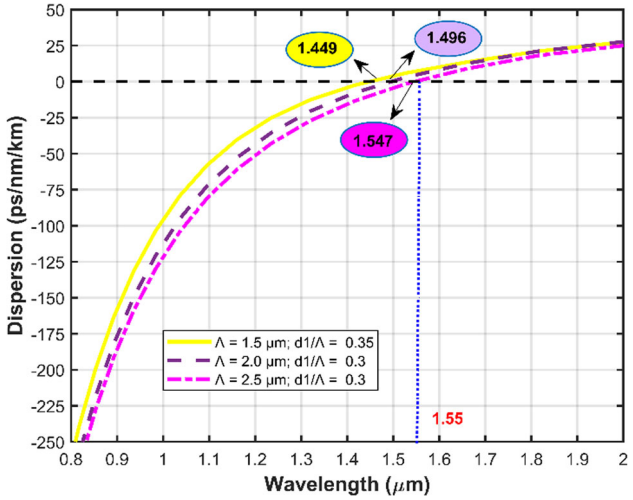

Fig. 6 Comparison of the PCFs with near-zero flat anomalous dispersion

conditions (Fig. 6). The dispersion curve of the fiber with $\Lambda = 2.5$ μm, $d_1/\Lambda = 0.3$ is flatter and closer to zero dispersion than the others. Additionally, this fiber has a ZDW at 1.547 μm, very close to the pump wavelength chosen in the third transmission window (1.55 μm) to minimize losses. These are two fibers $\#F_1$ and $\#F_2$ suggested earlier. Based on this, we further analyze the optical properties of the selected structures and calculate the values at the corresponding pump wavelengths. The results in Table 1 highlight our design by optimizing the dispersion characteristic when adjusting the diameter of the first air hole round, at the same time reducing the effective mode area after keeping the filling factor in the remaining rings up to the maximum value [27]. The publications [15, 16, 20, 21] use PCFs with the same air hole diameter parameter. Therefore, only the dispersion can be optimized, but not the effective mode area. This limits the nonlinearity of the PCFs.

5 SCG in optimized PCFs

For the SCG of the proposed fibers, we chose a commercially available erbium-fiber laser with the parameters of 1.3 μm, 40 fs for $\#F_2$, and 1.55 μm and 95 fs for $\#F_2$. SCG is reproduced at different peak input powers (P_0) when the fiber length is short, e. g 1 cm and 15 cm, to reduce costs and ignore loss. This has been mentioned in several publications [18, 20, 28].

The spectrum evolution for fiber $\#F_1$ with input power set in the range 0.075 to 0.45 kW is shown in Fig. 7. It is known that in the all-normal dispersion regime, SPM and OWB play a dominant role in SC spectral broadening. At low input power (0.075 kW), only SMP processes are present, hence the spectral broadening achieved is very limited. There exist many peaks of the spectrum caused by SPM, with the extreme peaks being the strongest. When the peak power increases (above 0.075 kW), the spectral broadening is influenced by the SPM at the beginning of propagation, after which the OWB appears at 0.9 μm wavelength when $P_0 = 0.225$ kW. As further increases the input power, this effect occurs at shorter wavelengths via FWM [24, 31]. The SC spectrum broadens over the wavelength range 0.72–1.76 μm (Fig. 7a).

Figure 7b, c shows continuous pulse expansion in the time domain. When $P_0 > 0.075$ kW, the SPM near the center wavelength produces an initial spectral growth. Then the onset of OWB broadens the spectrum of the wing significantly (Fig. 7b). The SPM-induced new short wavelength at the trailing edge is influenced by dispersion and travels slower at the center of the pulse than the pulse. The optical asymmetry that occurs in the shortwave range is based on self-steepening [36]. The OWB occurring at the trailing edge generates a new wavelength of about 0.72 μm after 0.37 cm propagation distance. The large dispersion slope at the pulse top limits spectral expansion at this edge during further propagating. This inhibits the wide effective modal range and high loss over the long wavelengths of 5 dB. Figure 7c depicts the temporal profile at various positions of the propagation length, respectively, with the spectrum growing along the fiber. The increase of input power causes the delay time between different frequencies to occur earlier at shorter propagation.

In addition to SPM and FWM, soliton fission (SF), and soliton self-frequency shift (SSFS), dispersive waves (DW) are also involved in spectral shaping in the anomalous regime of the dispersion. Using a 95 fs pulse launched into a 15 cm $\#F_2$ fiber, we obtain an ultra-broadband SC covering wavelengths from 0.8 to 3.95 μm at an input pulse value of 0.537 kW. The low material transmittance of C_6H_6 leads to a large absolute value of dispersion at short wavelength. At long wavelengths, the nonlinear coefficient is small. Therefore, the SC spectral structure changes with increasing pump peak power; however, the spectral bandwidth is assumed constant when the input peak power exceeds 0.116 kW. Besides, as shown in Fig. 8a, the complex temporal structure of pulses with very poor coherence properties sacrifices spectral bandwidth advantage.

Noise amplification is normally known as an active means of generating broadband spectra over an octave under pumping from a relatively simple laser. Modulation instability-induced noise would be declined if pumping in the normal and near-zero anomalous dispersion regions. Interestingly, SPM still predominates early in propagation. It undergoes normal dispersion conditions before SF occurs. SF already started appearing after 5 cm with the help of FWM, emitting a series of elementary solitons [37] under the influence of small perturbations. By increasing the pump power to its maximum value of 0.537 kW, a new wavelength band is created at the trailing edge under the large effect of the DW. Due to the dramatic optical propagation, SSFS shifts the fundamental soliton to the long-wavelength region. Thus, the spectrum is broaden significantly toward red light (Fig. 8b). For the time delay between different frequencies, it occurs earlier when

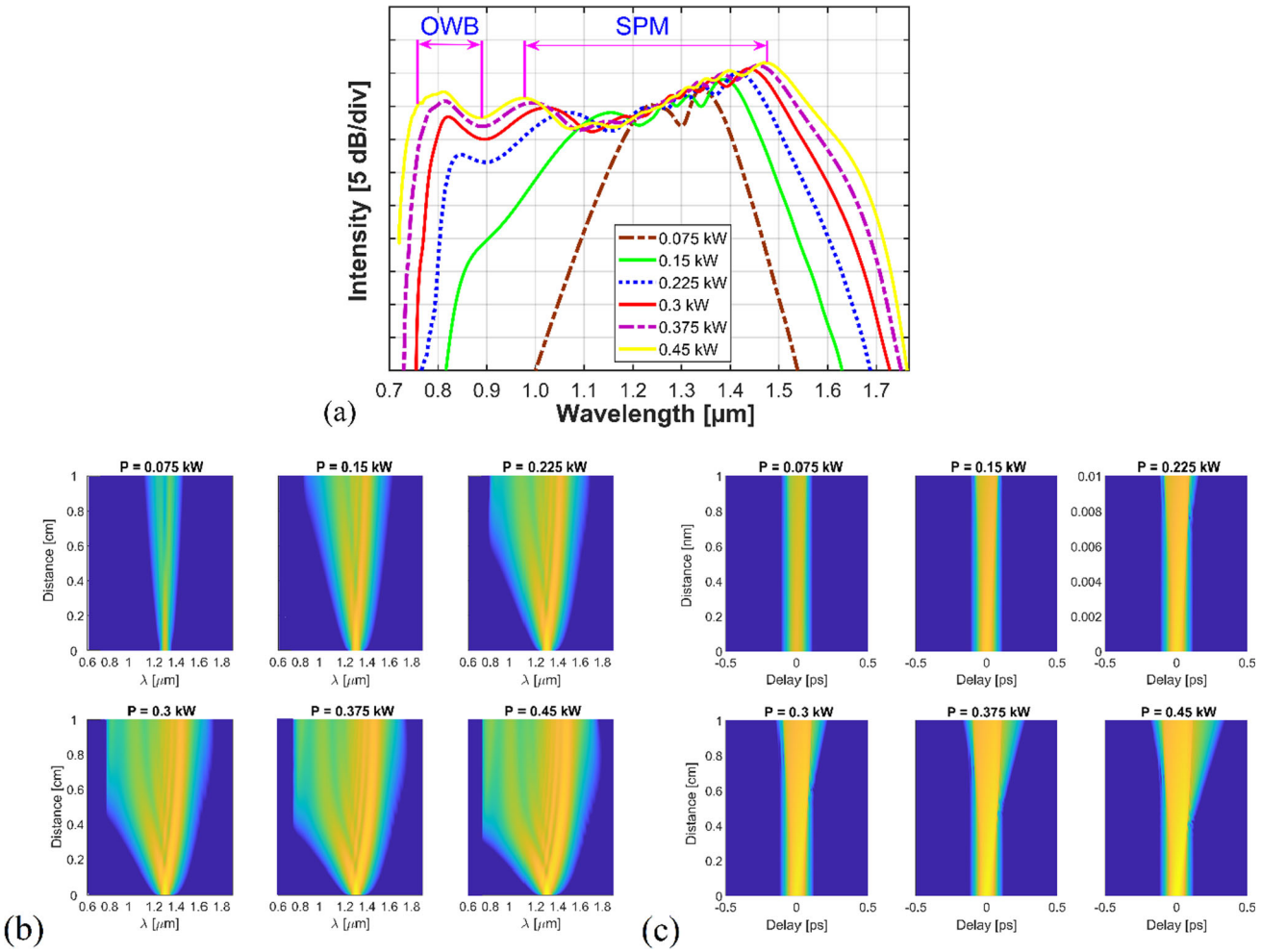

Fig. 7 **a** The output SC with various input powers in 1 cm #F_1 fiber, **b** the spectrum evolution, and **c** the temporal profile at different propagation lengths

the input pulse energy increases. Because of the difference in group velocity components, these values become larger with longer distances (Fig. 8c).

Based on a flexible combination of PCF design and careful selection of highly nonlinear liquids, dispersion and nonlinear properties of PCF are improved for broad and coherent SCG. The obtained broad SC spectrum in comparison with some previous publications is presented in Table 2. C_6H_6-PCFs in this work enable a broader SC spectrum with low peak power although n_2 of C_6H_6 is lower compared with carbon disulfide and is equivalent to nitrobenzene and toluene [18, 20]. With the same liquid-filled, the work [15] showed that the generated SC spectra were very broad of 1.3 μm for optimal fiber with all-normal dispersion, but the peak power was very high, at 55 kW. Similarly, with the high peak power, even 38 times higher than that used for #F_1 fiber, the publication [38] whose SC spectrum extends only 1.2 μm. Further, other publications [7, 18, 39] demonstrated the SCG ability of fibers with higher peak power than our fibers, but the SC spectrum width is only equivalent to that of #F_1 fiber. For an anomalous dispersion regime, the work [15] presented a very broad SC spectrum up to 2.9 μm but with peak power as large as 18.5 kW, more than 34 times the power used for #F_2 fiber. Although the peak power used for #F_1 and #F_2 fibers is equivalent to that of [18], their SC spectrum is broader.

6 Conclusion

Numerical modeling for SCG in square lattice C_6H_6-core PCFs is analyzed in detail with the support of NLSE. By adjusting the diameter of the first air hole ring, the PCF characteristics are simultaneously optimized for the small effective mode area, high nonlinearity, and flat near-zero dispersion. The influence of pump source parameters on the SC bandwidth was also considered. Simulations show that a smooth SC with a bandwidth of 1.04 μm can be successfully obtained for a 1 cm long #F_1 fiber at a peak input power of 0.45 kW.

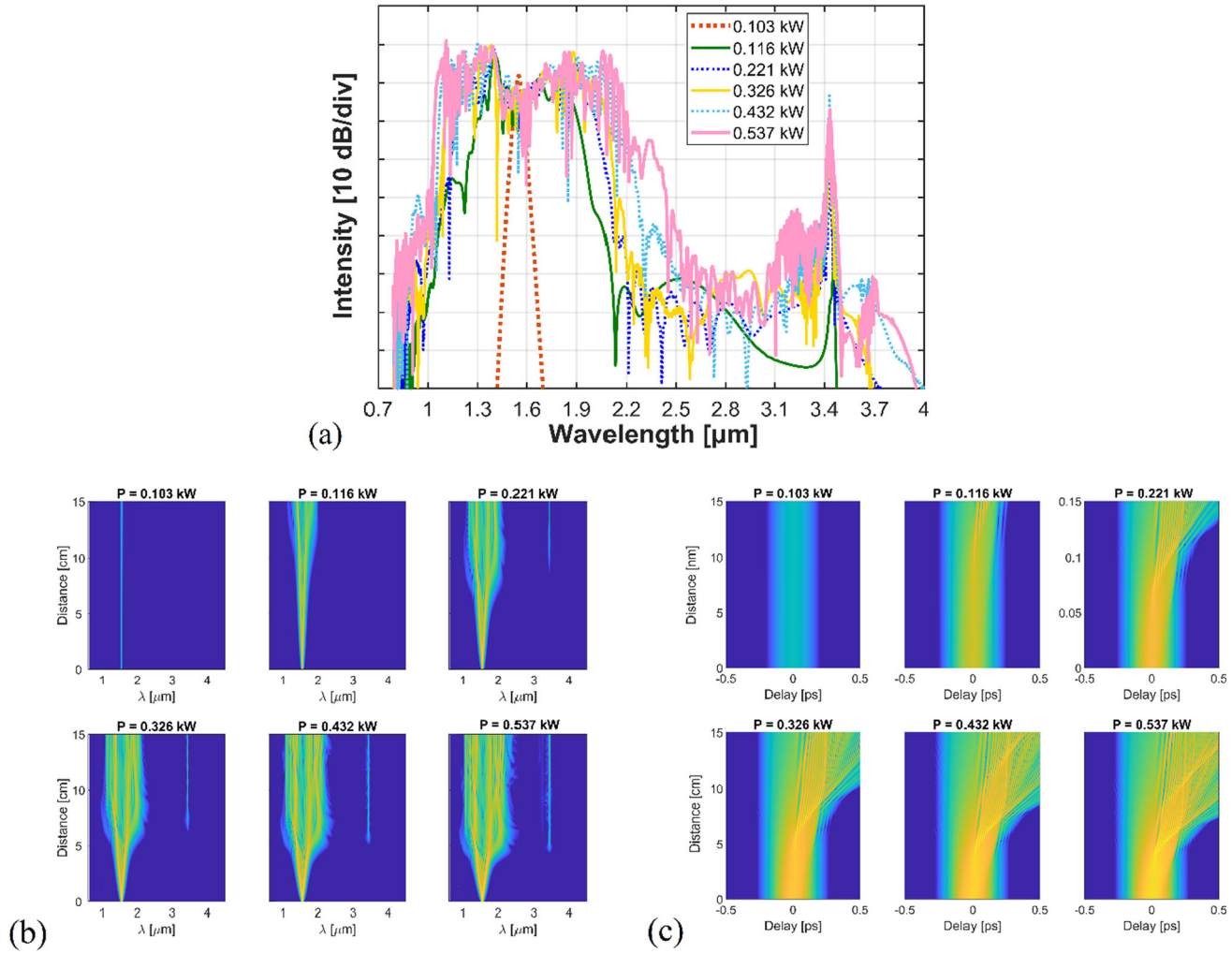

Fig. 8 **a** The output SC with various input powers in 15 cm #F_2 fiber, **b** the spectrum evolution, and **c** the temporal profile at different propagation lengths

Table 2 The spectral broadening of selected PCFs compared to other liquid-core PCFs

#	References	T_0 (fs)	P_0 (kW)	λ_p (μm)	Fiber length (cm)	Spectral width (μm)	Regime
$CHCl_3$	[7]	400	2.5	1.03	10	0.66	All-normal
$CHCl_3$	[7]	400	2	1.03	10	0.8	Anomalous
C_6H_6	[15]	90	55	1.56	1	1.3	All-normal
C_6H_6	[15]	90	18.5	1.56	1	2.9	Anomalous
C_7H_8	[18]	40	0.45	1.064	1	0.95	All-normal
C_7H_8	[18]	90	0.556	1.55	10	1.585	Anomalous
C_2Cl_4	[38]	90	16.67	1.56	5	1.2	All-normal
C_2Cl_4	[38]	90	5	1.56	10	1.0	Anomalous
CCl_4	[39]	400	2.67	1.064	30	0.2	All-normal
$C_6H_5NO_2$	[40]	90	5.55	1.56	5	1.3	All-normal
$C_6H_5NO_2$	[40]	90	0.66	1.56	5	1.0	Anomalous
#F_1	This study	40	0.45	1.3	1	1.04	All-normal
#F_2	This study	95	0.537	1.55	15	3.15	Anomalous

SCG in $\#F_2$ fiber covers more than two octaves (0.8 to 3.95 μm) at 15 cm length. Therefore, $\#F_2$ fiber is very useful for a wide-bandwidth spectrum, while $\#F_1$ has been proven suitable for several high pulse-to-pulse coherence applications. On the other hand, C_6H_6 also shows its advantage in maximizing spectral broadening and reducing peak input power. The proposed fiber-based low-cost compact all-fiber SC system is expected to be further extended in future commercial applications.

Acknowledgements Not applicable.

Authors' contributions

All authors contributed to the study conception and design. LCV contributed to conceptualization, methodology, writing—original draft, supervision, and writing—review and editing. BTLT contributed to writing—original draft, visualization, investigation, and data curation.

Funding No funding was received to assist with the preparation of this manuscript.

Data availability This manuscript has associated data in a data repository. [Authors' comment: No data was used for the research described in the article.]

Code availability Not applicable.

Declarations

Conflict of interest The authors have no relevant financial or non-financial interests to disclose.

References

1. M.B. Hossain, A.A.M. Bulbul, M.A. Mukit, E. Podde, Opt. Photonics J. **7**, 235 (2017)
2. H. Fu, D. Chen, Z. Cai, Sensors **12**, 5395 (2012)
3. A. Sharafali, N. Kanagaraj, Appl. Phys. B **126**, 55 (2020)
4. J.G. Porquez, R.A. Cole, A.D. Slepkov, OSA Contin. **1**, 1385 (2018)
5. K. Park, J. Na, J. Kim, Y. Jeong, IEEE J. Quantum Electron. **56**, 6800109 (2020)
6. J.M. Dudley, J.R. Taylor, *Supercontinuum Generation in Optical Fibers* (Cambridge University Press, England, 2010)
7. C.V. Lanh, H.V. Thuy, C.L. Van, K. Borzycki, D.X. Khoa, T.Q. Vu, M. Trippenbach, R. Buczyński, J. Pniewski, Laser Phys. **29**, 075107 (2019)
8. M.F.H. Arif, M.M. Hossain, N. Islam, S.M. Khaled, Sens. Bio-Sens. Res. **22**, 100252 (2019)
9. J. Vengelis, V. Jarutis, V. Sirutkaitis, Opt. Lett. **43**, 2571 (2018)
10. S. Kajla, S. Gupta, Int. J. Eng. Res. Technol. **3**, 2278 (2014)
11. Y.L. Tan, H.L. Wang, Y.R. Wang, Comput. Opt. **42**, 816 (2018)
12. L.T.B. Tran, D.V. Trong, C.V. Lanh, N.T.H. Phuong, T.N.M. Hang, H.T. Duc, N.T. Thuy, Dalat. Uni. J. Sci. **13**, 3 (2022)
13. M. Shanthi, R. Seyezhai, Plasmonics **15**, 525 (2020)
14. R.H. Jibon, A.A.M. Bulbul, M.E. Rahaman, Sens. Bio-Sens. Res. **32**, 100405 (2021)
15. C.V. Lanh, H.V. Thuy, C.L. Van, K. Borzycki, D.X. Khoa, T.Q. Vu, M. Trippenbach, R. Buczyński, J. Pniewski, Opt. Eng. **60**, 116109 (2021)
16. A.A. Nair, M. Jayaraju, Pramana J. Phys. **91**, 66 (2018)
17. P.S. Maji, P.R. Chaudhuri, J. Opt. Soc. Korea **18**, 207 (2014)
18. N.T. Thuy, H.T. Duc, L.T.B. Tran, D.V. Trong, C.V. Lanh, J. Opt. **51**, 678 (2022)
19. A. Sharafali, K. Nithyanandan, Appl. Phys. B **126**, 55 (2020)
20. C.V. Lanh, N.T. Thuy, H.T. Duc, L.T.B. Tran, V.T.M. Ngoc, D.V. Trong, L.C. Trung, H.D. Quang, D.Q. Khoa, Opt. Quant. Electron. **54**, 300 (2022)
21. C.V. Lanh, L.T.B. Tran, D.V. Trong, V.T.M. Ngoc, N.T. Thuy, N.T.H. Phuong, T.N.M. Hang, H.V. Thuy, Opt. Fiber Technol. **75**, 103151 (2023)
22. D.X. Khoa, C.V. Lanh, Comput. Phys. **22**, 343 (2012)
23. L. Liu, T. Cheng, K. Nagasaka, H. Tong, G. Qin, T. Suzuki, Y. Ohishi, Opt. Lett. **41**, 392 (2016)
24. T. Sylvestre, E. Genier, A.N. Ghosh, P. Bowen, G. Genty, J. Troles, A. Mussot, A.C. Peacock, M. Klimczak, A.M. Heidt, J.C. Travers, O. Bang, J.M. Dudley, J. Opt. Soc. Am. B **38**, F90 (2021)
25. M. Chemnitz, C. Gaida, M. Gebhardt, F. Stutzki, J. Kobelke, A. Tünnermann, J. Limpert, M.A. Schmidt, Opt. Express **26**, 3221 (2018)
26. *Market Study: Benzene*, 2nd edn. Ceresana. Accessed Oct 2 2015
27. K. Saitoh, M. Koshib, T. Hasegawa, E. Sasaoka, Opt. Express **11**, 843 (2003)
28. C.V. Lanh, L.T.B. Tran, N.T. Thuy, H.T. Duc, D.V. Trong, D.M. Trang, T.N. Hoang, T.D. Thanh, D.Q. Khoa, Opt. Quant. Electron **54**, 840 (2022)
29. G. Stepniewski, R. Kasztelanic, D. Pysz, R. Stepien, M. Klimczak, R. Buczyński, Opt. Mater. Express **6**, 2689 (2016)
30. S. Kedenburg, M. Vieweg, T. Gissibl, H. Giessen, Opt. Mater. Express **2**, 1588 (2012)
31. H.V. Thuy, R. Kasztelanic, A. Anuszkiewicz, G. Stepniewski, A. Filipkowski, S. Ertman, D. Pysz, T. Wolinski, D.X. Khoa, M. Klimczak, R. Buczyński, Opt. Mater. Express **8**, 3568 (2018)
32. J.M. Dudley, G. Genty, S. Coen, Rev. Mod. Phys. **78**, 1135 (2006)
33. M. Vieweg, T. Gissibl, S. Pricking, B.T. Kuhlmey, D.C. Wu, B.J. Eggleton, H. Giessen, Opt. Express **18**, 25232 (2010)
34. C.V. Lanh, L.V. Hieu, D.N. Nguyen, V.T.M. Ngoc, D. Quang, H.V. Thuy, N.T. Thuy, C.V. Bien, Laser Phys. **32**, 055102 (2022)
35. D. Pysz, I. Kujama, R. Stepién, M. Klimczak, A. Filipkowski, M. Franczyk, L. Kociszewski, J. Buźniak, K. Haraśny, R. Buczyński, Bull. Pol. Acad. Sci. Tech. Sci. **62**, 667 (2014)
36. H. Saghaei, Radioengineering **26**, 16 (2017)

37. C.S. Cheung, M. Spring, H. Liang, Opt. Express **23**, 10145 (2015)
38. L.V. Hieu, H.V. Thuy, N.T. Hue, C.L. Van, R. Buczyński, R. Kasztelanic, Opt. Quant. Electron **53**, 187 (2021)
39. H.D. Quang, J. Pniewski, L.V. Hieu, A. Ramaniuk, C.L. Van, K. Borzycki, D.X. Khoa, M. Klimczak, R. Buczyński, Appl. Opt. **57**, 3738 (2018)
40. C.V. Lanh, H.V. Thuy, K. Borzycki, D.X. Khoa, T.Q. Vu, M. Trippenbach, R. Buczyński, J. Pniewski, Laser Phys. **30**, 035105 (2020)